Computational Materials Science 110 (2015) 115–120

Contents lists available at ScienceDirect

Computational Materials Science

journal homepage: www.elsevier.com/locate/commatsci

Effect of exchange–correlation on first-principles-driven lattice thermal conductivity predictions of crystalline silicon

Ankit Jain, Alan J.H. McGaughey *

Department of Mechanical Engineering, Carnegie Mellon University, Pittsburgh, USA

ARTICLE INFO

Article history:
Received 2 June 2015
Received in revised form 7 August 2015
Accepted 8 August 2015

Keywords:
Thermal conductivity
Density functional theory
Lattice dynamics
Boltzmann transport equation
Pseudopotentials
Phonons

ABSTRACT

The effects of exchange–correlation (XC) and pseudopotential types on the density functional theory-driven prediction of the thermal conductivity of isotopically pure silicon are studied. The thermal conductivity is predicted by considering three-phonon scattering processes and a full solution of the Boltzmann transport equation. The LDA, PBE, PBEsol, and PW91 XCs predict thermal conductivities between 127 and 148 W/m K at a temperature of 300 K, which is an under-prediction of the experimental value of 153 W/m K by 3–17%. The BLYP XC predicts a thermal conductivity of 172 W/m K, an over-prediction of 12%.

1. Introduction

The prediction of lattice thermal conductivity from first-principles-driven density function theory (DFT) calculations is becoming routine [1–4]. As opposed to using empirical potentials to describe the atomic interactions, which require fitting parameters and lack true predictive power, DFT-driven calculations are fitting-parameter free. DFT-driven calculations have been successfully used to predict the experimentally-measured thermal conductivities of materials ranging from simple semiconductors such as silicon [2] and diamond [5] to compound semiconductors [4], graphene [6], and SiGe alloys [3]. DFT-driven calculations have also been used to study the effects of strain and isotopes on the thermal conductivity of semiconductors [7–9] and to predict the thermal conductivity of novel two-dimensional materials [6,10,11].

Within the framework of DFT, the many-body problem of interacting electrons is reduced to a tractable problem of non-interacting electrons with an effective potential. This effective potential includes the effects of the Coulombic interactions (i.e., the Hartree term) and many-body interactions [i.e., the exchange–correlation (XC) term]. The major challenge in DFT lies in describing the XC. The simplest form of the XC is the local density approximation (LDA), in which the potential is only a function of the spatially-dependent electron density [12]. A more involved approach, the generalized gradient approximation (GGA), uses the electron density and its gradient. GGA XCs almost always over-predict the experimental lattice constants of crystalline solids while LDA XCs almost always result in an under-prediction [13]. The effect of this under-/over-binding by different XCs on lattice thermal conductivity is unknown.

Thermal transport in semiconducting and electrically insulating crystalline solids is dominated by lattice vibrations (i.e., phonons). The thermal conductivity of these materials is therefore highly-dependent on inter-atomic separation and bonding. Our objective here is to study the effect of different XCs on the thermal conductivity of isotopically-pure silicon. We employ LDA and GGA (PBE [14], PBEsol [15], BYLP [16,17], and PW91 [18]) XC-based ultrasoft (US), norm-conserving (NC), and projected augmented wave (PAW) pseudopotentials. We find that all XCs, with the exception of BYLP, predict a thermal conductivity between 127 and 148 W/m K at a temperature of 300 K, which is an under-prediction of the experimental value of 153 W/m K by 3–17% [19]. BLYP, on the other hand, over-predicts the experimental value by 12%. In what follows, we describe the thermal conductivity calculation details in Section 2 and convergence tests for the DFT calculations in Section 3. The predictions of the XC-dependence of thermal conductivity are presented in Section 4 and a comparison to results from the literature is made in Section 5.

* Corresponding author.
E-mail address: mcgaughey@cmu.edu (A.J.H. McGaughey).

http://dx.doi.org/10.1016/j.commatsci.2015.08.014
0927-0256/

2. Thermal conductivity

The phonon contribution to the thermal conductivity of a bulk crystalline solid in the l direction can be calculated by solving the Boltzmann transport equation (BTE) iteratively and using the Fourier law and is [4,20]

$$k_l = \sum_i c_{ph,i} v_{g,l,i}^2 \tau_{l,i}. \quad (1)$$

The summation in Eq. (1) is over all the phonon modes in the first Brillouin zone. The mode index, $i \equiv \begin{pmatrix} \boldsymbol{\kappa} \\ \nu \end{pmatrix}$, enumerates phonon wave vector, $\boldsymbol{\kappa}$, and polarization, ν. On the right-hand side of Eq. (1), $c_{ph,i}$ is the volumetric specific heat, $v_{g,l,i}$ is the l-component of the phonon group velocity vector $\mathbf{v}_{g,i}$, and $\tau_{l,i}$ is the phonon lifetime. The phonon volumetric specific heat can be calculated using the Bose–Einstein distribution as

$$c_{ph,i} = \frac{k_B x^2}{V} \frac{e^x}{[e^x - 1]^2}, \quad (2)$$

where $x \equiv \hbar\omega_i / k_B T$, k_B is the Boltzmann constant, $\hbar$ is the reduced Planck constant, T is temperature, and V is the system volume. The group velocity vector is related to the mode frequency, $\omega_i \equiv \omega_\nu^{\boldsymbol{\kappa}}$, as $\mathbf{v}_{g,i} = \partial\omega_\nu^{\boldsymbol{\kappa}} / \partial\boldsymbol{\kappa}$. The phonon lifetimes can be estimated using the inverse of the phonon scattering rate as $\tau_{l,i} = \frac{1}{\partial n_{l,i}/\partial t}$ [20–22].

3. DFT parameters convergence

Phonon frequency and lifetime predictions require harmonic and cubic force constants as inputs. We obtained harmonic force constants from density functional perturbation theory (DFPT) and cubic force constants from finite differencing of DFT forces. We employed the planewave-based electronic-structure calculation package Quantum Espresso for our DFPT and DFT calculations [23,24]. The harmonic force constants are initially obtained on an $8 \times 8 \times 8$ phonon wave-vector grid and are later interpolated to a $24 \times 24 \times 24$ grid. For the cubic force constants, we calculated forces on different arrangements of a 216 atom supercell with one or more atoms displaced by 0.01 Å from their equilibrium positions. The translational invariance constraint in the calculation of the cubic force constants was enforced using the Lagrangian approach presented by Li et al. [25]. The convergence of the thermal conductivity of silicon with respect to supercell size and displacement amount is discussed in Ref. [4]. We found that the change in thermal conductivity at a temperature of 300 K is less than 1.5% when increasing the phonon wave-vector grid from $24 \times 24 \times 24$ to $26 \times 26 \times 26$. Since we want our results to be converged within 2% (the experimental uncertainty in the thermal conductivity of silicon [19]), we used the $24 \times 24 \times 24$ phonon wave-vector grid for all of our calculations. The phonon scattering rates in the present study are obtained using an iterative solution of the BTE. The iterative solution, as opposed to the commonly-used relaxation time approximation (RTA), does not treat normal three-phonon scattering processes as resistive [1,26].

To specify the converged electronic wave vector grid (to be used in the self-consistent field calculation), we plot the variation of the total energy, the relaxed lattice constant, and the thermal conductivity at a temperature of 300 K with electronic wave-vector grid density in Fig. 1(a) and (b) for the LDA XC-based NC pseudopotential with a 60 Ry planewave energy cutoff. As can be seen in Fig. 1(b), the thermal conductivity decreases by 7% on increasing the electronic wave-vector grid from $6 \times 6 \times 6$ to $8 \times 8 \times 8$ and is converged to within 1.5% with further increase. The 7% decrease in the thermal conductivity in going from the $6 \times 6 \times 6$ wavevector grid to the $8 \times 8 \times 8$ wavevector grid is mainly a result of differences in the vibrational frequencies. For example, the transverse (longitudinal) acoustic phonon group velocities close to the Gamma point in the [100] direction decrease from 4806 m/s (7871 m/s) to 4653 m/s (7558 m/s). The changes in the total energy per atom and the relaxed lattice constant (Fig. 1(a)) are less than 0.2 mRy and 0.001 Å with an increase in an electronic wave-vector grid beyond $8 \times 8 \times 8$. These results suggest that the total energy per atom and the lattice constant should be converged to within 0.2 mRy and 0.001 Å in order to achieve a converged thermal conductivity for silicon (within 2%). We note that the 7% variation in the thermal conductivity with electronic wavevector grid is not simply because of the change in the lattice constant. We performed thermal conductivity calculations using lattice constants between 5.40 and 5.46 Å while keeping the electronic wavevector grid and planewave energy cutoff fixed and found the variation to be less than 4%.

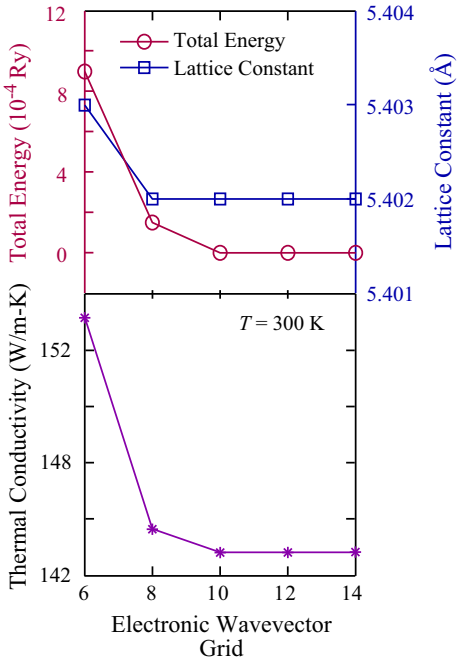

Fig. 1. Variation of (a) total energy and relaxed lattice constant and (b) predicted thermal conductivity of silicon at a temperature of 300 K with electronic wave-vector grid using the LDA XC-based NC pseudopotential. The total energy in (a) is energy per atom relative to energy per atom of the $14 \times 14 \times 14$ electronic wave-vector grid.

We repeated the above convergence calculations for all the XCs with the criterion of thermal conductivity changes of less than 2%. The converged electronic wave-vector grid obtained for all XCs and pseudopotential types is $8 \times 8 \times 8$. For the planewave energy cutoff, we find convergence at 50 Ry for US and PAW pseudopotentials and 60 Ry for NC pseudopotentials for all of the XCs considered. To see the effect of electronic wavevector grid on the supercell DFT forces (used for both the phonon lifetimes and the Grüneisen parameters), we calculated thermal conductivity using the Gamma point supercell and a supercell with a $2 \times 2 \times 2$ wave vector grid for the LDA XC-based NC pseudopotential. The difference in the two thermal conductivities is 2%, which is within our convergence threshold.

4. Results

4.1. Lattice constant

We report the relaxed lattice constants in Table 1. The experimental value is 5.430 Å [27]. All GGA XCs under-bind the lattice

and over-predict the lattice constant while the opposite is true for the LDA XC, which underpredicts by 0.6%. The PBEsol XC-predicted lattice constant (5.430 Å) shows the best agreement with the experimental value while the BLYP XC over-predicts the experimental value by the highest amount (1.4%). The PBE and PW91 lattice constants are within 0.7% of the experimental value for the three types of pseudopotential considered.

4.2. Phonon dispersion

We plot the phonon dispersion calculated using the PBEsol (US) and BLYP (NC) XCs in Fig. 2(a). As mentioned in Section 4.1, the PBEsol and BLYP predicted lattice constants show the best and worst agreement with the experimental value. The transverse acoustic phonon vibrational frequencies predicted using PBEsol (green lines) are lower than the experimental values (blue circles [28]), whereas those predicted using BLYP (red lines) are higher. For longitudinal acoustic phonons, both PBEsol and BLYP predict similar vibrational frequencies. In the case of optical phonons, the PBEsol predicted frequencies agree well with the experiments whereas BLYP results in an under-prediction. The sound velocities (estimated as the longitudinal acoustic phonon velocity close to the Γ-point in the [100] direction) from the PBEsol (8330 m/s) and BLYP (8510 m/s) XCs both compare well with the experimental value of 8430 m/s [30].

The sound velocities obtained using the different XCs and pseudopotential types are provided in Table 1. PW91 underpredicts the sound velocity compared to the experimental value by the maximum amount (5970 m/s, a difference of 29%). The sound velocities predicted from the other XCs and pseudopotential types are within 11% of the experimental value. The sound velocity of a one-dimensional harmonic mass-spring chain in solids is $a\sqrt{\frac{K}{m}}$, where $a, K,$ and m are the lattice constant, the harmonic spring constant, and the atomic mass. In examining Table 1, we note that there is not a direct correlation between the sound velocities and the lattice constants. For example, for the LDA XCs, the predicted sound velocities are 8320, 7560, and 8340 m/s from the US, NC, and PAW pseudopotentials even though all predicted lattice constants are within 0.002 Å of each other. This finding points to the important effect of the XC on the harmonic force constants.

4.3. Three-phonon phase space

Differences in the phonon dispersions from the different XC and pseudopotential types result in different values of the three-phonon phase space, which is a measure of the scattering space available for three-phonon processes. It is calculated using the phonon dispersion by counting the number of three-phonon scattering processes that satisfy the energy and momentum conservation selection rules [31]. The three-phonon phase spaces obtained from the different XC and pseudopotential types are provided in Table 1. The minimum phase spaces are obtained from BLYP and PW91, with values of 0.0085 and 0.0089. All other XC and pseudopotential types predict values between 0.0091 and 0.0093. These results indicate a smaller number of three-phonon scattering processes from the BLYP and PW91 XCs as compared to the other XCs. We note that the strength of these three-phonon scattering processes depends on the cubic force constant and is discussed in Section 4.4.

4.4. Grüneisen parameters

To examine the effect of XC and pseudopotential types on the cubic force constants, we next plot mode-dependent Grüneisen parameters, γ_i, calculated using the PBEsol (NC) and BLYP (US) XCs in Fig. 2(b). The Grüneisen parameters describe the effect of changing the crystal volume on the phonon frequencies and are a measure of crystal anharmonicity. We calculated the Grüneisen parameters with the cubic force constants by using Eq. (2) of Ref. [32]. For transverse acoustic phonons, PBEsol results in an over-prediction (in magnitude) of the experimentally measured Güneisen parameter [29] at all of the high-symmetry points considered. BLYP, on the other hand, matches the experimental values at Γ and W, while under-predicting (in magnitude) at X and L by a factor of two. The Grüneisen parameters for the transverse acoustic phonons from BLYP are smaller in magnitude (less than half in some cases) than the corresponding values from PBEsol over the entire Brillouin zone. This result suggests weaker anharmonic scattering of transverse acoustic phonons from BLYP compared to PBEsol. For longitudinal acoustic and optical phonons, except for the $\Gamma - L$ direction, the BLYP- and PBEsol-predicted Grüneisen parameters match with each other in all high-symmetry directions. Both the BLYP- and PBEsol-predicted Grüneisen parameters match with the experiments at all of the high-symmetry points for longitudinal acoustic and optical phonons.

We characterize the anharmonicity of the different XCs by calculating an average Grüneisen parameter, γ, as a heat-capacity weighted average of the absolute values of the mode-dependent Grüneisen parameters as:

$$\gamma \equiv \frac{\sum_i C_{ph,i}|\gamma_i|}{\sum_i C_{ph,i}}. \quad (3)$$

The average Grüneisen parameters are provided in Table 1. The minimum value of 0.89 (i.e., the least anharmonic) is obtained from the BLYP XC. All other XCs and pseudopotential types result in average Grüneisen parameter values between 1.00 and 1.11.

4.5. Thermal conductivity

Thermal conductivities at a temperature of 300 K calculated using the different XC and pseudopotential types are provided in Table 1. The maximum and minimum predicted thermal conductivities are 127 W/m K (from PW91) and 172 W/m K (from BLYP). All other XCs predict values between 137 and 148 W/m K, which is an under-prediction of the experimentally-measured thermal conductivity of isotopically pure silicon of 153 W/m K [19] by 3–11%. As can be seen from Eq. (1), thermal conductivity is proportional to the phonon group velocities squared and the lifetimes. The strong under-prediction of the sound velocity by PW91 (Section 4.2) is consistent with its low thermal conductivity. For BLYP XC, the three-phonon phase space and average Grüneisen parameter are lower than the other XCs. These lower values of the three-phonon phase space and average Grüneisen parameter are an indication of weaker phonon–phonon scattering, larger phonon lifetimes, and hence higher thermal conductivity. Apart from the XC and pseudopotential types, the predicted thermal conductivities also depend on the pseudopotential generation method, as found by Ward for diamond [33]. We find the predicted thermal conductivities from the LDA XC based NC pseudopotentials generated using the Goedecker–Hartwigsen–Hutter–Teter [34,35], Martins–Troullier [36], and Von Barth-Car [37] methods to be 130, 134, and 144 W/m K.

The thermal conductivity accumulation function with phonon mean free path (defined as $\tau_i|\mathbf{v}_{g,i}|$) at a temperature of 300 K from the different XC and pseudopotential types is plotted in Fig. 3. The accumulation function describes the contribution of different mean free path phonons towards the thermal conductivity [38]. As can be seen from Fig. 3, phonons with mean free paths varying over three orders of magnitude (10 nm to 10 μm) contribute to

Table 1
Predicted relaxed lattice constant, sound velocity, three-phonon phase space, mode-averaged Grüneisen parameter, and phonon thermal conductivity (isotopically pure at $T = 300$ K) of silicon with different XCs and pseudopotential types. The thermal conductivities are converged to within 2% with respect to all simulation parameters.

Pseudopotential type [24]	Exchange correlation [24]	Lattice constant (Å)	Sound velocity (m/s)	Three-phonon phase space (arbitrary units)	Average Grüneisen parameter	Thermal conductivity (W/m K)
Experiment		5.430 [27]	8430 [30]			153 [19]
Ultrasoft	LDA	5.399	8320	0.0091	1.11	142
	PBE	5.468	8120	0.0092	1.04	148
	PBEsol	5.430	8330	0.0092	1.10	140
	PW91	5.466	5970	0.0089	1.00	127
Norm-conserving	LDA	5.402	7560	0.0092	1.04	144
	PBE	5.461	8150	0.0093	1.02	148
	BLYP	5.505	8510	0.0085	0.89	172
PAW	LDA	5.400	8340	0.0091	1.11	142
	PBE	5.466	7830	0.0092	1.03	145
	PBEsol	5.430	8320	0.0092	1.11	137

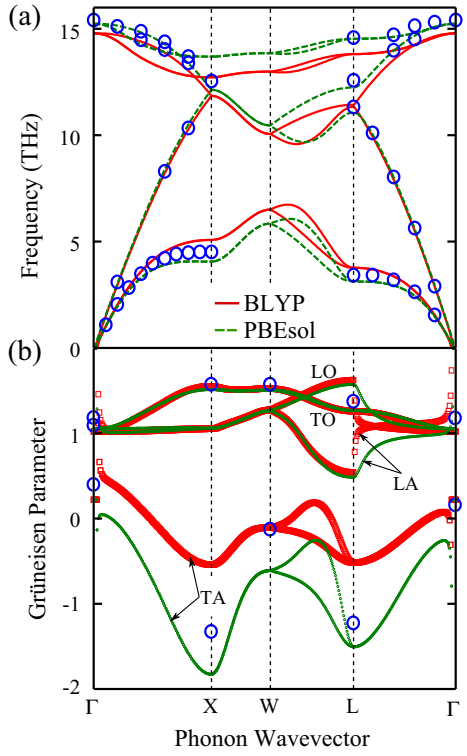

Fig. 2. (a) Phonon dispersion and (b) mode-dependent Grüneisen parameters of silicon calculated using the BLYP XC NC pseudopotential (red) and the PBEsol XC US pseudopotential (green). Experimentally measured frequencies from Ref. [28] and Grüneisen parameters from Ref. [29] are shown using blue circles. LA, TA, LO, and TO in (b) represents longitudinal acoustic, transverse acoustic, longitudinal optical, and transverse optical. (For interpretation of the references to colour in this figure legend, the reader is referred to the web version of this article.)

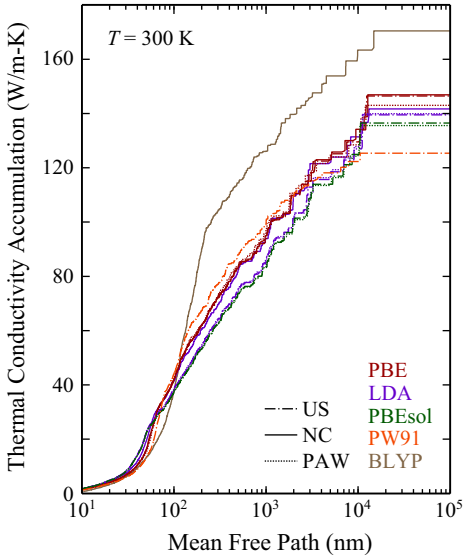

Fig. 3. Thermal conductivity accumulation function of silicon at a temperature of 300 K from different XC and pseudopotential types. With the exception of BLYP, all XCs result in a similar accumulation.

thermal transport. As compared to the other XCs, which show similar accumulations, BLYP over-predicts the contribution of the mid-range mean free path (~100 nm) phonons.

The temperature variation of the thermal conductivity of silicon between 100 and 500 K from different XC and pseudopotential types is plotted in Fig. 4. Also plotted are the experimentally-measured thermal conductivities from Inyushkin et al. [19] (green) and Glassbrenner and Slack [39] (red). BLYP over-predicts the experimental thermal conductivity at all of the temperatures considered. At a temperature of 100 K, BLYP predicts a value of 1326 W/m K, while all other XC and pseudopotential types predict values between 993 and 1239 W/m K. The experimental values at a temperature of 100 K are 1194 and 950 W/m K from Refs. [19,39].

5. Comparison with literature

We now compare our predictions with reported values in literature. The results are summarized in Table 2. As a comparison point, our converged value of thermal conductivity using the LDA XC based NC pseudopotential is 144 W/m K using the iterative solution of the BTE and 140 W/m K when the BTE is solved under the RTA.

Lindsay et al. [4] predicted a value of 155 W/m K using an iterative solution of the BTE. They used the LDA XC based NC pseudopotential with a $6 \times 6 \times 6$ electronic wavevector grid and a 80 Ry planewave energy cutoff. Using the same parameters, our predicted thermal conductivity is 153 W/m K [42]. As can be seen from Fig. 1(b), an electronic wavevector grid of $6 \times 6 \times 6$ is not converged and leads to a 6% over-prediction in the thermal conductivity compared to an $8 \times 8 \times 8$ wavevector grid.

Esfarjani et al. [2] predicted a value of 132 W/m K using the LDA XC and the RTA of the BTE. They used a 40 Ry planewave energy cutoff and 10 electronic wavevectors in the irreducible Brillouin zone ($4 \times 4 \times 4$ wave-vector grid) of a 64 atom supercell. They used a $18 \times 18 \times 18$ phonon wavevector grid for the thermal conductivity calculation [43]. These choices lead to an under-prediction of thermal conductivity (compared to finer phonon wavevector grids) due to insufficient sampling of phonon modes

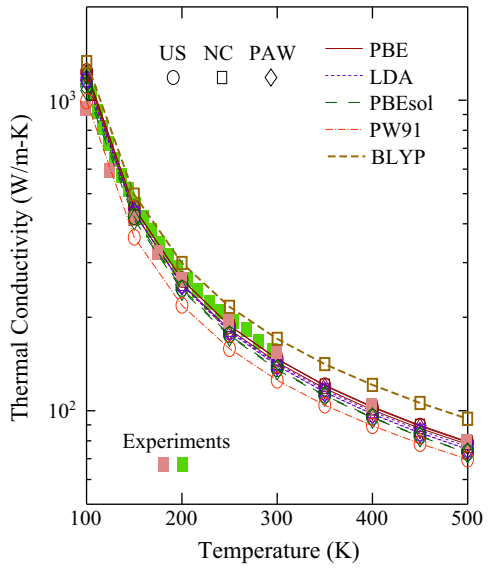

Fig. 4. Thermal conductivity variation of silicon with temperature from different XC and pseudopotential types. The experimentally measured thermal conductivities from Refs. [19,39] are shown as green and pink filled squares. (For interpretation of the references to colour in this figure legend, the reader is referred to the web version of this article.)

near the Brillouin zone center [2,44]. Using the LDA XC based NC pseudopotential and their parameters we predict a thermal conductivity of 136 W/m K.

The thermal conductivity predicted by Garg et al. [40] is 136 (132) W/m K using the full (RTA) solution of the BTE. They used the LDA XC-based NC pseudopotential with an $8 \times 8 \times 8$ electronic wavevector grid and a 20 Ry planewave energy cutoff. With the same parameters, we predict thermal conductivities of 140 (136) W/m K. These value are an under-prediction of our converged values by 4 W/m K (for both cases) due to an insufficient planewave energy cutoff.

Li et al. [41] predicted the thermal conductivity of silicon to be 172 W/m K using an iterative solution of the BTE and the PBE XC based PAW pseudopotential. They used a 23 Ry planewave energy cutoff and calculated harmonic (cubic) force constants on a $5 \times 5 \times 5$ ($3 \times 3 \times 3$) supercell using Γ-point DFT calculations. The harmonic force constants calculated on a $5 \times 5 \times 5$ supercell using Γ-point DFT calculations are equivalent to those from DFPT calculations with $5 \times 5 \times 5$ phonon and electronic wavevector grids. Using the PAW XC based PBE pseudopotential, $5 \times 5 \times 5$ phonon and electronic wavevector grids in the DFPT calculations, and a $3 \times 3 \times 3$ supercell for DFT force calculations, we obtain a thermal conductivity of 140 W/m K, which differs from prediction of Li et al. by 32 W/m K. We hypothesize that Li et al.'s use of DFT forces to extract the harmonic force constants (as opposed to the more accurate DFPT calculations in the present study) is responsible for this difference between the two results.

Parrish et al. [9] predicted a thermal conductivity of 151 W/m K using an iterative solution of the BTE, the LDA XC based NC pseudopotential, and a 80 Ry planewave energy cutoff with a $6 \times 6 \times 6$ electronic wavevector grid. This value is an overestimate of our converged value by 5% due to an insufficient electronic wavevector grid.

The thermal conductivity of silicon has also been predicted by Broido et al. [1] and Ward et al. [33]. Their values are 155 and 145 W/m K using LDA-based US and Bachelet-Hamann-Schlüter (BHS)-based NC pseudopotentials. Because the DFPT phonon wavevector grid for the harmonic force constant calculation is not provided in Ref. [1] and the BHS based NC pseudopotential in not available in Quantum Espresso [23], we are unable to compare our prediction methodology with theirs.

6. Summary

We studied the effect of DFT parameters and XC and pseudopotential types on the thermal conductivity of isotopically pure silicon. We found that the total energy per atom and relaxed lattice constant should be converged to within 0.2 mRy and 0.001 Å with respect to all DFT parameters in order to have a 2% convergence in the thermal conductivity. Furthermore, we identified that with the exception of BLYP (which over-predicts by 12%), all other XCs under-predict the experimental thermal conductivity by 3–17% at a temperature of 300 K.

Our conclusions are for isotopically pure silicon. We recommend a careful selection of XC and pseudopotential types for other materials by initially checking the sound velocity and Grüneisen parameters, which can both be obtained with harmonic-level calculations. While some XCs such as LDA and PBE are developed for condensed matter, other XCs are developed for chemical energy calculations of molecules (e.g., BLYP). We also recommend a careful convergence of thermal conductivity with all DFT parameters, especially electronic wave-vector grid and planewave energy cutoff.

Acknowledgment

We thank K. D. Parrish and J. A. Malen (Carnegie Mellon University) for their helpful discussions.

References

[1] D.A. Broido, M. Maloney, G. Birner, N. Mingo, D. Stewart, Appl. Phys. Lett. 91 (2007) 231922, http://dx.doi.org/10.1063/1.2822891.

Table 2
Comparison of isotopically-pure silicon thermal conductivity predictions at a temperature of 300 K between the present study and previous results.

	Relevant/Unconverged simulation parameters	Thermal conductivity (W/m K)	Our thermal conductivity prediction with same parameters (W/m K)
Present study	Iterative (RTA) solution of the BTE with LDA NC pseudopotential, $8 \times 8 \times 8$ electronic wave-vector grid, 60 Ry planewave energy cutoff, and $24 \times 24 \times 24$ phonon wave-vector grid	144 (140)	
Lindsay et al. [4]	Iterative solution of the BTE with $6 \times 6 \times 6$ electronic wave-vector grid	155	153
Esfarjani et al. [2]	RTA solution of the BTE and $18 \times 18 \times 18$ phonon wave-vector grid	132	136
Garg et al. [40]	Iterative (RTA) solution of the BTE and 20 Ry planewave energy cutoff	136 (132)	140 (136)
Li et al. [41]	Iterative solution of the BTE with $5 \times 5 \times 5$ supercell based Γ-point DFT calculations for harmonic force constants using PBE based PAW pseudopotential	172	140
Parrish et al. [9]	Iterative solution of the BTE with $6 \times 6 \times 6$ electronic wave-vector grid	151	153
Broido et al. [1]	Iterative solution of the BTE with LDA based US pseudopotential	155	
Ward et al. [33]	Iterative solution of the BTE with BHS-based NC pseudopotential	145	

[2] K. Esfarjani, G. Chen, H.T. Stokes, Phys. Rev. B 84 (2011) 085204, http://dx.doi.org/10.1103/PhysRevB.84.085204.
[3] J. Garg, N. Bonini, B. Kozinsky, N. Marzari, Phys. Rev. Lett. 106 (2011) 045901, http://dx.doi.org/10.1103/PhysRevLett.106.045901.
[4] L. Lindsay, D.A. Broido, T.L. Reinecke, Phys. Rev. B 87 (2013) 165201, http://dx.doi.org/10.1103/PhysRevB.87.165201.
[5] A. Ward, D.A. Broido, D.A. Stewart, G. Deinzer, Phys. Rev. B 80 (12) (2009) 125203, http://dx.doi.org/10.1103/PhysRevB.80.125203.
[6] L. Lindsay, W. Li, J. Carrete, N. Mingo, D.A. Broido, T.L. Reinecke, Phys. Rev. B 89 (2014) 155426, http://dx.doi.org/10.1103/PhysRevB.89.155426.
[7] L. Lindsay, D.A. Broido, T.L. Reinecke, Phys. Rev. Lett. 109 (2012) 095901, http://dx.doi.org/10.1103/PhysRevLett.109.095901.
[8] S. Mukhopadhyay, D.A. Stewart, Phys. Rev. Lett. 113 (2014) 025901, http://dx.doi.org/10.1103/PhysRevLett.113.025901.
[9] K.D. Parrish, A. Jain, J.M. Larkin, W.A. Saidi, A.J.H. McGaughey, Phys. Rev. B 90 (2014) 235201, http://dx.doi.org/10.1103/PhysRevB.90.235201.
[10] W. Li, J. Carrete, N. Mingo, Appl. Phys. Lett. 103 (2013) 253103, http://dx.doi.org/10.1063/1.4850995.
[11] A. Jain, A.J.H. McGaughey, Sci. Rep. 5 (2015), http://dx.doi.org/10.1038/srep08501.
[12] W. Kohn, L.J. Sham, Phys. Rev. 140 (1965) A1133–A1138, http://dx.doi.org/10.1103/PhysRev.140.A1133.
[13] L. He, F. Liu, G. Hautier, M.J.T. Oliveira, M.A.L. Marques, F.D. Vila, J.J. Rehr, G.-M. Rignanese, A. Zhou, Phys. Rev. B 89 (2014) 064305, http://dx.doi.org/10.1103/PhysRevB.89.064305.
[14] J.P. Perdew, K. Burke, M. Ernzerhof, Phys. Rev. Lett. 77 (1996) 3865–3868, http://dx.doi.org/10.1103/PhysRevLett.77.3865.
[15] J.P. Perdew, A. Ruzsinszky, G.I. Csonka, O.A. Vydrov, G.E. Scuseria, L.A. Constantin, X. Zhou, K. Burke, Phys. Rev. Lett. 100 (2008) 136406, http://dx.doi.org/10.1103/PhysRevLett.100.136406.
[16] A.D. Becke, Phys. Rev. A 38 (1988) 3098–3100, http://dx.doi.org/10.1103/PhysRevA.38.3098.
[17] C. Lee, W. Yang, R.G. Parr, Phys. Rev. B 37 (1988) 785–789, http://dx.doi.org/10.1103/PhysRevB.37.785.
[18] J.P. Perdew, J.A. Chevary, S.H. Vosko, K.A. Jackson, M.R. Pederson, D.J. Singh, C. Fiolhais, Phys. Rev. B 46 (1992) 6671–6687, http://dx.doi.org/10.1103/PhysRevB.46.6671.
[19] A.V. Inyushkin, A.N. Taldenkov, A.M. Gibin, A.V. Gusev, H.-J. Pohl, Physica Status Solidi (c) 1 (2004) 2995–2998.
[20] J.A. Reissland, The Physics of Phonons, John Wiley and Sons Ltd, 1973.
[21] J.E. Turney, E.S. Landry, A.J.H. McGaughey, C.H. Amon, Phys. Rev. B 79 (2009) 064301.
[22] D.C. Wallace, Thermodynamics of Crystals, Cambridge Univ. Press, Cambridge, UK, 1972.
[23] P. Giannozzi, S. Baroni, N. Bonini, M. Calandra, R. Car, C. Cavazzoni, D. Ceresoli, G.L. Chiarotti, M. Cococcioni, I. Dabo, A.D. Corso, S. de Gironcoli, S. Fabris, G. Fratesi, R. Gebauer, U. Gerstmann, C. Gougoussis, A. Kokalj, M. Lazzeri, L. Martin-Samos, N. Marzari, F. Mauri, R. Mazzarello, S. Paolini, A. Pasquarello, L. Paulatto, C. Sbraccia, S. Scandolo, G. Sclauzero, A.P. Seitsonen, A. Smogunov, P. Umari, R.M. Wentzcovitch, J. Phys-Condens. Mat. 21 (39) (2009) 395502, http://dx.doi.org/10.1088/0953-8984/21/39/395502.
[24] The pseudopotentials files used in this study are, in the order provided in Table 1: Si.pz-n-rrkjus_psl.0.1.UPF, Si.pbe-n-van.UPF, Si.pbesol-n-rrkjus_psl.0.1.UPF, Si.pw91-n-van.UPF, Si.pz-vbc.UPF, Si.pbe-hgh.UPF, Si.blyp-hgh.UPF, Si.pz-n-kjpaw_psl.0.1.UPF, Si.pbe-n-kjpaw_psl.0.1.UPF, and Si.pbesol-n-kjpaw_psl.0.1.UPF.
[25] W. Li, L. Lindsay, D.A. Broido, D.A. Stewart, N. Mingo, Phys. Rev. B 86 (2012) 174307, http://dx.doi.org/10.1103/PhysRevB.86.174307.
[26] M. Omini, A. Sparavigna, Phys. Rev. B 53 (1996) 9064–9073.
[27] C. Kittel, Introduction to Solid State Physics, 6th ed., John Wiley & Sons, Inc., New York, 1986.
[28] G. Nilsson, G. Nelin, Phys. Rev. B 6 (10) (1972) 3777–3786, http://dx.doi.org/10.1103/PhysRevB.6.3777.
[29] Silicon (Si), Gruneisen parameters and related data, in: O. Madelung, U. Rossler, M. Schulz (Eds.), Group IV Elements, IV–IV and III–V Compounds. Part b – Electronic, Transport, Optical and Other Properties, Vol. 41A1b of Landolt-Bornstein – Group III Condensed Matter, Springer Berlin Heidelberg, 2002, pp. 1–6.
[30] M. Hopcroft, W. Nix, T. Kenny, J. Microelectromechan. Syst. 19 (2) (2010) 229–238, http://dx.doi.org/10.1109/JMEMS.2009.2039697.
[31] L. Lindsay, D.A. Broido, J. Phys.: Condens. Matter 20 (16) (2008) 165209. http://stacks.iop.org/0953-8984/20/i=16/a=165209.
[32] J. Fabian, P.B. Allen, Phys. Rev. Lett. 79 (1997) 1885–1888, http://dx.doi.org/10.1103/PhysRevLett.79.1885.
[33] A.N. Ward, First principles theory of the lattice thermal conductivity of semiconductors, PhD Thesis, Boston College, 2009.
[34] S. Goedecker, M. Teter, J. Hutter, Phys. Rev. B 54 (1996) 1703–1710, http://dx.doi.org/10.1103/PhysRevB.54.1703.
[35] C. Hartwigsen, S. Goedecker, J. Hutter, Phys. Rev. B 58 (1998) 3641–3662, http://dx.doi.org/10.1103/PhysRevB.58.3641.
[36] N. Troullier, J.L. Martins, Phys. Rev. B 43 (1991) 1993–2006, http://dx.doi.org/10.1103/PhysRevB.43.1993.
[37] A. Dal Corso, S. Baroni, R. Resta, S. de Gironcoli, Phys. Rev. B 47 (1993) 3588–3592, http://dx.doi.org/10.1103/PhysRevB.47.3588.
[38] C. Dames, G. Chen, Thermoelectrics Handbook: Macro to Nano, CRC press, 2005. Ch. 42, pp. 42–1–42–11.
[39] C.J. Glassbrenner, G.A. Slack, Phys. Rev. 134 (1964) A1058–A1069, http://dx.doi.org/10.1103/PhysRev.134.A1058.
[40] J. Garg, N. Bonini, N. Marzari, in: S.L. Shinde, G.P. Srivastava (Eds.), Length-Scale Dependent Phonon Interactions, Topics in Applied Physics, Vol. 128, Springer, New York, 2014, pp. 115–136.
[41] W. Li, J. Carrete, N.A. Katcho, N. Mingo, Comput. Phys. Commun. 185 (6) (2014) 1747–1758, http://dx.doi.org/10.1016/j.cpc.2014.02.015. http://www.sciencedirect.com/science/article/pii/S0010465514000484.
[42] We note that our predicted lattice constant is 5.403 Å, as opposed to the 5.37 Å reported by Lindsay et al. [4] using the same simulation parameters. We further note that, as mentioned in Section 3, a 0.03 Å difference in the lattice constant does not have a significant effect on the thermal conductivity.
[43] Following the approach described by Esfarjani et al. [2], a further increase in thermal conductivity by 10 W/m K is expected due to contributions from long wavelength phonons that are not captured in the $18 \times 18 \times 18$ phonon wavevector gird.
[44] A. Jain, Y.-J. Yu, A.J.H. McGaughey, Phys. Rev. B 87 (2013) 195301, http://dx.doi.org/10.1103/PhysRevB.87.195301.